Theoretical Chemistry Accounts (2022) 141:43
https://doi.org/10.1007/s00214-022-02902-9

REGULAR ARTICLE

Role of non-covalent interactions in deciding the fate of product formation in bifunctional thiourea-assisted chiral organic reactions

Parimal J. Maliekal[1] · Nitin Gulvi[1] · Purav M. Badani[1]

Received: 5 February 2022 / Accepted: 25 July 2022 / Published online: 2 August 2022

Abstract

The present work reports the theoretical study of the reaction between anthrones and maleimides organocatalyzed by bifunctional thiourea. It has been observed that the substituents attached to the reactant determine the reaction path, which in turn induces the formation of different products. Our mechanistic study has explored the various possible routes for the product formation. We observed that the non-covalent interactions specifically the N–H···O and C–H···O play a decisive role in deciding the fate of stereoselectivity of the products. The formation of favoured/disfavoured products is accounted on the basis of energy profiling. The reaction results in outstanding yields and enantioselectivities of Diels–Alder cycloadduct when *N*-phenylmaleimide is used as dienophile (99% ee, RR configuration), whereas Michael adduct is formed as a major product on using *N*-(4-trifluoromethylphenyl)maleimide (99% ee, S configuration). These theoretically obtained results are in line with the experimentally observed values. The difference in the reactant stimulates the variation in the interactions, and these insights can eventually aid the experimentalists to design subsequent experiments in the future.

Keywords Diels–Alder · Michael addition · Enantioselectivity · Energy barrier · Transition state · Organocatalysis

1 Introduction

Organocatalysts have embarked a new paradigm in synthetic methodology attributing to its ability of forming hydrogen bonds [1]. The innate capability of forming hydrogen bonds and to orient a favourable spatial arrangement has proven entities such as squaramides [2], guanidinium ions [3], and (thio)ureas [4–6], to be promising catalyst structures [7]. Takemoto introduced chiral bifunctional catalysts possessing a 3,5-bis(trifluoromethyl)phenyl group which increases the acidic character of the thiourea, thus enhancing its ability of hydrogen bonding (HB) [8]. It has emerged as one of the dominant systems in number of organocatalytic moieties for inducing chirality.

In particular, thiourea-based amines have indeed been proved efficient as multifunctional organocatalysts in asymmetric Michael addition (MA), Diels–Alder (DA) reaction, Mannich reaction, Henry reaction, Strecker reaction, MBH reaction, and related annulations [9, 10]. Zea et al. have reported an engrossing study on bifunctional thiourea chiral catalysed reaction between anthrone and maleimide in present of toluene as the solvent, as shown in Scheme 1. The key observation of their work was that the substituent attached on a moiety solely plays a decisive role in altering the fate of products [11]. The presence of phenyl as a substituent on maleimide favours the formation of R,R—DA product (90% ee), whereas *N*-(4-trifluoromethylphenyl) maleimide provides the S—MA (97% ee). The calibre of substituents to cause a variance in chiral product formation intrigued us to compute the reaction mechanism of DA and MA reactions.

Computational chemistry has turned out essential to study the course of reaction since it provides information on the reactivity of the species at each step, allowing researchers to adjust the entities for future study. Our prior research focused on the effect of organocatalysts on product enantioselectivity, and in this study we are delighted to investigate the effect of substituents connected to a reactant, which thus leads to the formation of different products [12]. Herein, we highlight the significant factors, asserting the energetically feasible route through which the organocatalytic species relate to the intermediate bearing negatively charged oxygen which are stabilized by the non-covalent interactions. A

✉ Purav M. Badani
pmbadani@chem.mu.ac.in

[1] Department of Chemistry, University of Mumbai, Vidyanagari Santacruz, Mumbai 400098, India

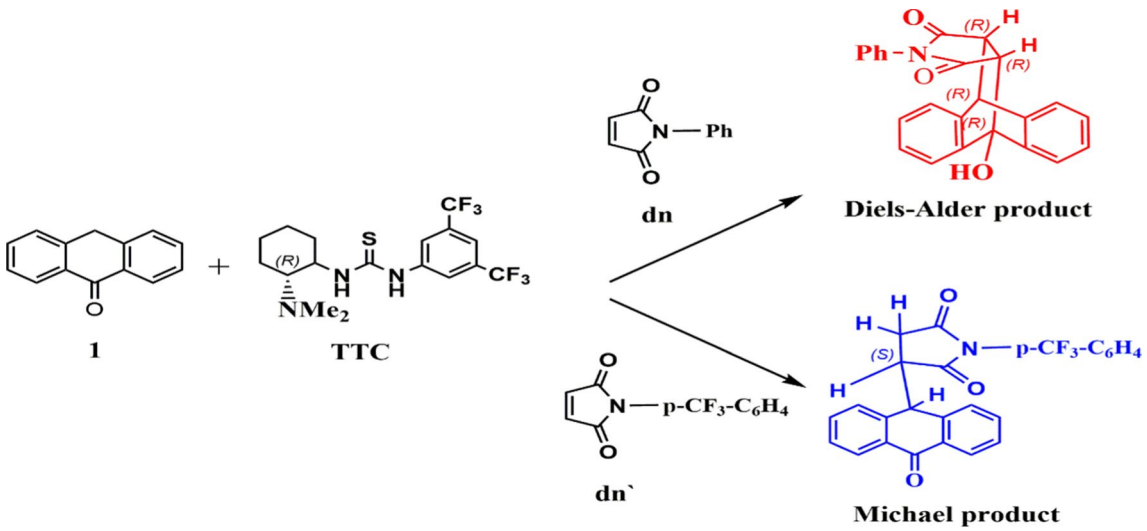

Scheme 1 Enantioselective reaction between anthrone (**1**) and N-phenylmaleimide (**dn**)/N-(4-trifluoromethyl phenyl)maleimide (**dn`**) organocatalysed by Takemoto thiourea catalyst (**TTC**) resulting in the formation of Diels–Alder and Michael adduct

simultaneous donation of two (or more) hydrogen bonds and the presence of C–H···O / N–H···O interaction has caused these systems to be highly influential in determining the stereoselectivity of the reaction [7, 13, 14]. Our in-depth mechanistic examination elucidates the experimental findings, and the computed enantioselectivity is in well agreement with the observed results. The work reported in this paper should be helpful for explaining the role of substituents and thus be fruitful for the rational design of precursors for organic synthesis.

2 Methodology

The geometry optimization of the entities involved in the current work was performed using the Gaussian 09 program [15]. The B3LYP functional along with a basis set 6-31+G(d,p) has been found reliable in estimating the geometries for the MA and DA reactions [16–22]. Houk and coworkers further demonstrated that Minnesota functional (M06) provides reliable energies of reactant, TSs, intermediates and products of organic species [23]. Hence, in order to obtain reliable geometries and energies we have performed computations at M06-2X/6-31+G(d,p)//B3LYP/6-31G and B3LYP/6-31+G(d,p)//B3LYP/6-31G level of theory [24–27]. In addition, the influence of the solvent was confirmed in the toluene environment by performing single-point electronic structure calculations at the same level employing an implicit CPCM model [28]. The stability of the entities at the ground state was ascertained by the absence of imaginary frequencies, while the transition structures were defined by the existence of a single imaginary frequency. The obtained transition structures were subjected to intrinsic reaction coordinate (IRC) scan, thereby ensuring the connectivity between the reactant and the intermediate/product [29, 30]. The Cartesian coordinates of all the structures are presented in the SI.

3 Results and discussion

3.1 Analysing the most basic site in the bifunctional thiourea organocatalyst

The Takemoto thiourea consists of three nitrogen atoms, and so, in order to examine their basicity we calculated the proton affinities of each nitrogen atom. [20]. The proton affinity calculations were performed in both gas phase and solvent phase, the values of which are listed in Table S1. These computationally evaluated values enable us to infer the following facts that the lone pair of electrons contained in 16 N and 20 N undergo electron delocalization and thus possess relatively less electron density as compared to the 36 N atom present as tertiary amine whose lone pair of electrons are readily available [31]. The nitrogen and sulphur atoms of the thioamide group are sp^2 hybridized, and so, the sp^3 hybridized nitrogen (36 N) present in the tertiary amine acts as the basic site available for protonation. The two methyl groups attached on the nitrogen, through their + I effect, enhance the basicity of 36 N. The basicity has also been checked by mapping the total electron density on the organocatalyst through molecular electrostatic potential map (MEP) [32]. The highly positive electrostatic potential is indicated by red colour, and so from Figure S1 we can conclude that 36 N is the most basic site of the organocatalyst.

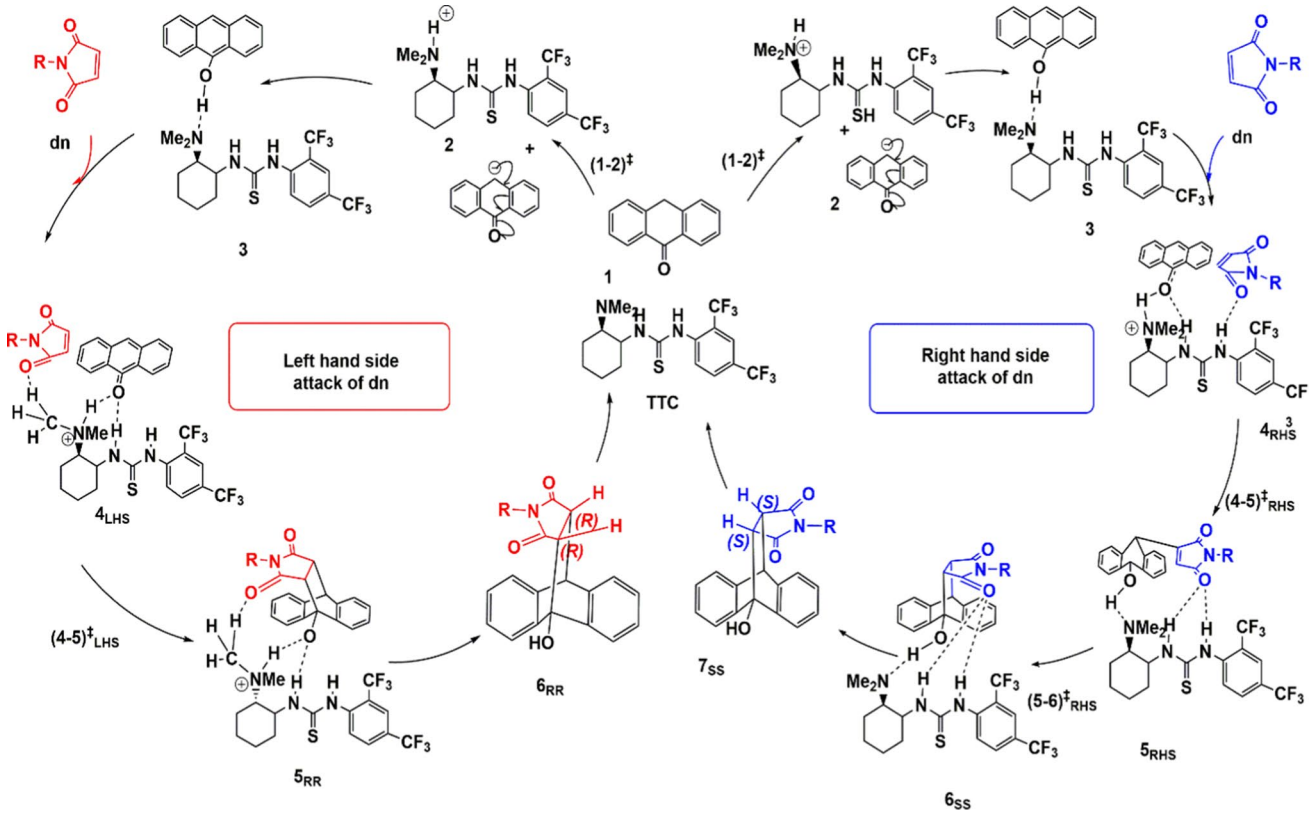

Scheme 2 A Mechanized asymmetric Diels–Alder reaction between **1** and **dn** catalysed by **TTC**

3.2 Reaction of anthrone and *N*-phenylmaleimide assisted by Takemoto thiourea catalyst

3.2.1 Energy profiling of the reaction between anthrone and N-phenylmaleimide

The possible mechanism of the reaction catalysed by Takemoto thiourea (**TTC**) between anthrone (**1**) and N-phenylmaleimide (**dn**) is shown in Scheme 2. Figures S2, S3 and S4 of the SI provide the optimized structures of **1**, **dn** and **TTC** in the gas phase displayed in green, blue and red, respectively, for better visualization. The N atom present as tertiary amine, N36, of **TTC** abstracts the acidic proton of **1**. Eventually, it leads to the formation of **2** through the transition state $\mathbf{(1–2)}^{\ddagger}$ with an energy barrier of 20.3 kcal/mol (see Figures S5, S6 and S7a). The oxy-anion form of **1** eventually exhibits charge migration. The charge analysis was studied through ChelpG and NBO [33]. Compared to the deprotonated carbon, the oxygen atom of the deprotonated **1** had a higher negative charge indicating high electron density from initial −0.69 to −0.72 (see Figure S8 and Table S2 of SI). Consequently, deprotonated **1** experiences a dipole–dipole interaction with the protonated **TTC**, resulting in **3** with 25.7 kcal/mol stabilization energy (see Figure S9 of SI). The **dn** can bind to **3** either from the right-hand side or the left-hand side, resulting in $\mathbf{4_{RHS}}$ and $\mathbf{4_{LHS}}$, respectively (see Figure S10 and S11 of SI). It is primarily anticipated that these conformers will be stabilized through hydrogen bonding (HB) between the catalyst hydroxyl group and **dn**.

The stabilization energy of conformer $\mathbf{4_{RHS}}$ is 11.6 kcal/mol, whereas $\mathbf{4_{LHS}}$ was stabilized by 2.0 kcal/mol. This can be due to the difference in the binding mode, the **dn** in $\mathbf{4_{RHS}}$ exhibits N–H···O bonding with O···H having a bond length of 1.84 Å (see Figure S10), whereas in $\mathbf{4_{LHS}}$ the **dn** is far away from the thioamido group, and so, instead of forming N–H···O bonding, it shows the presence of C–H···O interaction as **dn** is closer to the methyl group adjacent to the protonated N36 (as presented in Scheme 2) [12]. In general, C–H···O hydrogen bonds stimulated by ammonium cations have evolved as a significant interaction for drug design [14]. $\mathbf{4_{LHS}}$ possesses a short C–H···O contact with a distance between H···O of 2.22 Å (see Figure S11), i.e. 0.38 Å shorter than the typical van der Waals separation (i.e. 2.6 Å) [13]. The HB length of 1.84 Å in $\mathbf{4_{RHS}}$ can be considered as a moderate HB and that of 2.22 Å HB in $\mathbf{4_{LHS}}$ as a weak HB, in accordance to the values reported by Rozas [34]. Therefore, $\mathbf{4_{RHS}}$ showed greater stability owing to N–H···O compared to $\mathbf{4_{LHS}}$ in the present case. The interconversion of the two conformers above is supposed to be simple as it has to cross the rotational barrier alone that is less than the

reaction activation energy [35]. It is also important to notice that, as per Brinck and coworkers, there is a decrease in the energy of the LUMO of **dn** if an organocatalyst binds to the electron-withdrawing group (EWG) of **dn** [36]. In the present case, due to the interaction of catalyst with **dn**, we also experienced a reduction of LUMO energy by 15.8 kcal/mol. We have also analysed the global reactivity indexes (ω) of the reactants in this key cycloaddition process so as to deeply analyse the position of the catalyst. The global molecule electrophilicity character is summarized in Table S3 of SI, which shows an elevation of ω to 2.61 eV [37, 38]. The nucleophilic carbon atom 51C (−0.542) of intermediate **4** shows a higher local electron density in comparison to 52C (0.175) (see Table S4 of SI) and subsequently attacks 75C of **dn** via **(4–5)**‡. The electronic energy barrier is estimated to be 8.7 kcal/mol for **(4–5)**$^{\ddagger}_{\mathbf{RHS}}$ and 5.7 kcal/mol for **(4–5)**$^{\ddagger}_{\mathbf{LHS}}$ (see Figure S12 and S13 of SI).

The LHS pathway shows an asynchronous concerted mechanism, with the first C–C bond having 2.07 Å and the second C–C bond having 2.98 Å, thus resulting in the formation of the cycloadduct $\mathbf{5_{RR}}$. On the other hand, the RHS pathway exhibits a stepwise mechanism and forms the SS cycloadduct (Scheme S1 of SI). Despite several attempts, we could not locate a concerted transition step for the RHS pathway. The intermediate $\mathbf{5_{RHS}}$ has more electron density at 76C. The mechanism therefore reveals a clear pathway indicating a nucleophilic attack of the **dn** moiety on the 52C atom of **1** to form the cycloadduct product $\mathbf{6_{SS}}$. The activation barrier for this step was equivalent to 1.13 kcal/mol. This reaction step was highly exothermic, indicating the generation of a stable product. The catalyst is detached from the cycloadduct with an additional energy of ~ 20 kcal/mol and becomes usable for the next reaction cycle. The potential energy surface (PES) for the current gas-phase reaction of interest is displayed in Fig. 1. The experiment was carried out in presence of several solvents and the best enantioselectivity was observed in toluene; therefore, we carried out energy estimations of the above reaction, in toluene as implicit solvent model using CPCM model [11]. The PES for the same is shown in Figure S21 of SI. The PES for the calculations performed at B3LYP functional, in gas phase as well as in solvent phase is shown in Figure S22 and S23 of SI, respectively. Small differences in the absolute energies of reactants, intermediates and products were seen, but the general trend in relative energies was similar.

In addition to the DA cycloadduct formation, the reaction can also proceed down to the formation of the MA. The compound acting as dienophile can now be referred to as Michael acceptors and the corresponding diene as Michael donor [39]. The entire steps till the formation of $\mathbf{5_{RHS}}$ are same, and then instead of undergoing C–C coupling as seen in DA mechanism, here, the nucleophile shows a 1,4-addition to an α,β-unsaturated carbonyl compound and results into MA with R chirality, i.e. **6*** through **(5–6)**$^{\ddagger *}$(See Scheme S2).The energy profile diagrams of the entire calculations carried out at B3LYP functional and M06-2X in both gas phase and solvent phase is presented in Fig. 2. When we compare the mechanism of DA and MA formation, we observe the difference begins from intermediate **5**. Intermediate **5** of DA follows the second C–C coupling, whereas in MA formation, intermediate **5** follows the de-protonation step. So, it is this particular step that decides the preferable

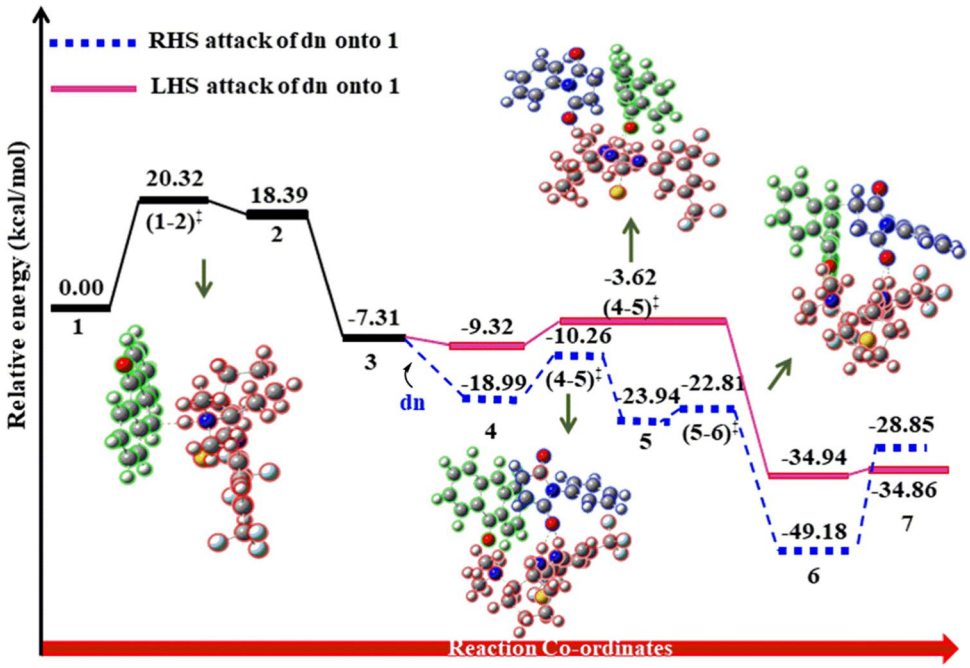

Fig. 1 Potential energy surface for DA reaction process between **1** and **dn** supported by **TTC** using electronic energies in the gas phase. The black solid line represents the energies for **dn**'s right-hand side attack, and the dotted blue line shows **dn**'s left-hand side attack energies

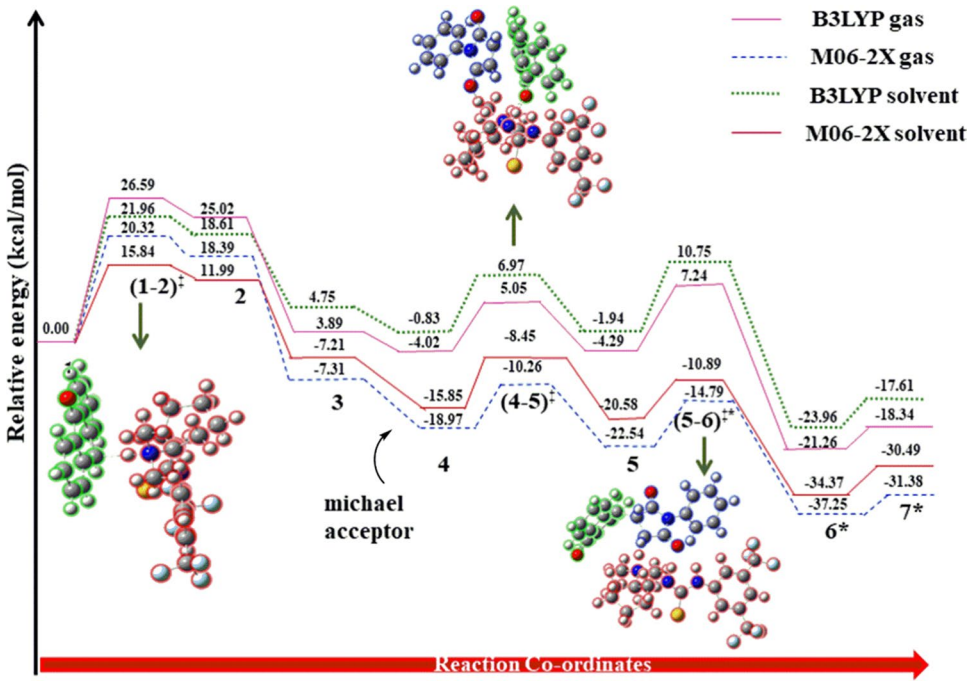

Fig. 2 A potential energy surface for Michael addition reaction between **1** and **Michael acceptor** supported by **TTC** using electronic energies. The pink solid line and green dotted line represent the energies estimated using B3LYP functional (in gas phase and solvent phase, respectively), and the blue dotted line and brown solid line represent the energies estimated using M062X functional (in gas phase and solvent phase, respectively)

formation of the specific products. Figure 1 reflects that for DA reaction, 1.1 kcal/mol of electronic energy is required for this step, and Fig. 2 shows that 7.7 kcal/mol of electronic energy is required to proceed for MA formation. Thus, it can be concluded that the mechanism which requires less energy will be favoured and so, DA product is formed as the major product when **dn** is used.

There is also a possibility of MA formation through retro synthesis. The tertiary amine of the catalyst abstracts the proton from DA cycloadduct $\mathbf{7}_{SS}$ and then forms the MA, $\mathbf{10}_{S}$ as shown in Scheme S3. The energy profile diagrams of the entire calculations for retro synthesis carried out at B3LYP functional and M06-2X in both gas phase and solvent phase are presented in Fig. 3. We observed that the DA product reverses its stereochemistry on forming the Michael product. Figure 3 indicates that the DA product (**6**) is much stable as compared to the MA (**10**). Thus, there is preferential formation of DA products as compared to the MA. This is in line with the experimental findings wherein DA product is formed when N-phenylmaleimide is used as the dienophile.

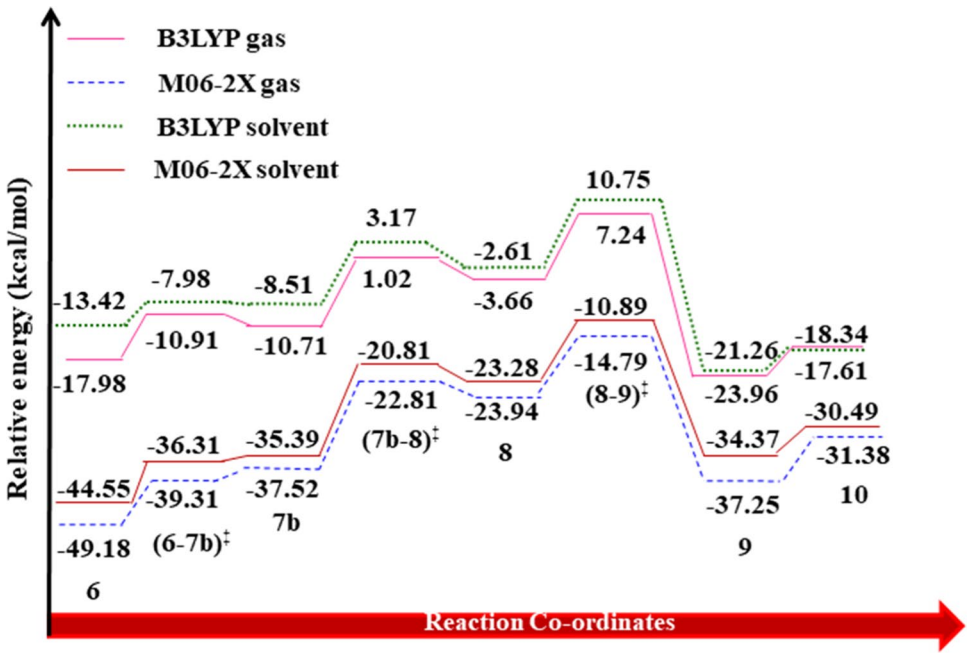

Fig. 3 Energy estimations for Michael addition through retro synthesis (R conformer). The pink solid line and green dotted line represent the electronic energies estimated using B3LYP functional (in gas phase and solvent phase, respectively), and the blue dotted line and brown solid line represent the energies estimated using M06-2X functional (in gas phase and solvent phase, respectively)

3.2.2 Stereo-chemical insights of the Diels–Alder reaction with N-phenylmaleimide

The fourth step of the reaction decides the stereo-chemical fate due to the specific interaction. As discussed in earlier section, $\mathbf{4_{RHS}}$ and $\mathbf{4_{LHS}}$ in general will contribute to the formation of products with SS and RR configurations, respectively, in accordance with the Curtin-Hammett theory [40]. As mentioned earlier, since the rotational barrier for interconversion between these two conformers is less than the activation energy of the proceeding reaction step, $\mathbf{4_{RHS}}$ will be converted into $\mathbf{4_{LHS}}$ and subsequently the reaction will progress further. The estimated *%ee* values calculated using M06-2X functional in the solvent phase matches very well with the experimental values previously recorded, as 90% being observed [11, 41], which are shown in Table 1.

3.3 Reaction of anthrone and *N*-(4-trifluoromethylphenyl)maleimide (dn`) assisted by Takemoto thiourea catalyst

3.3.1 Energy profiling of the reaction between anthrone and *N*-(4-trifluoromethylphenyl)maleimide

The entire reaction was checked in the presence of another dienophile i.e. *N*-(4-trifluoromethylphenyl)maleimide (**dn`**). The chiral entity with $-CF_3$ in **dn`** reported in this study provides the modulation of the steric environment [1]. The presence of $-CF_3$ group develops repulsive forces, thus rearranging the orientation of the reacting molecules, and thus these conformers show the presence of C–H···O interaction in both $\mathbf{4`_{RHS}}$ and $\mathbf{4`_{LHS}}$. The reaction mechanism is similar to that of the previous one. The charge analysis of the compounds is shown in Table S5. The IRC of the C–C coupling step obtained through $\mathbf{(4–5)`^{\ddagger}_{RHS}}$ and $\mathbf{(4–5)`^{\ddagger}_{LHS}}$ is shown in Figure S41. The energy profile diagrams of the entire calculations carried out at M06-2X functional and B3LYP in both gas phase and solvent phase are presented in Figures S45, S46, S47 and S48. It can be seen from Figure S45 that the LHS pathway leading to the formation of RR product requires 4.9 kcal/mol and the RHS pathway resulting in the formation of SS product requires 9.2 kcal/mol. The RR product is favoured in the formation of DA product.

As seen in the previous mechanism with **dn**, the reaction with **dn`** can also result in the formation of MA. The electronic energy barrier for the formation of $\mathbf{(5–6)^{\ddagger}`_{RHS}}$ is 1.1 kcal/mol, while LHS pathway leading to the formation of RR adduct requires 8.9 kcal/mol, and thus the RHS pathway leading to the formation of SS MA is favoured as seen in Figure S49. On comparing the mechanism of DA and MA formation, since the difference begins from intermediate **5,** this particular step decides the preferable formation of the specific products. Figure S45 reflects that for DA reaction, 2.5 kcal/mol of electronic energy is required for this step and Figure S49 shows that 1.1 kcal/mol of electronic energy is required to proceed for MA formation. Thus, it can be concluded that the MA is formed as the major product when **dn`** is used. The presence of three electron-withdrawing fluorine groups in **dn`** thus makes the proton highly acidic, thereby making it feasible for the de-protonation to form the MA rather than forming the C–C coupling which leads to DA product.

3.3.2 Stereo-chemical insights of the Michael adduct formation with *N*-(4-trifluoromethylphenyl) maleimide

As seen in previous case, the stereo-chemical outcome is defined in the fourth step of the reaction. We evaluated the energy required for MA formation using **dn`** which now behaves as the Michael acceptor. The $\Delta G^{\neq}_{RHS}$ of 7.2 kcal/mol and $\Delta G^{\neq}_{LHS}$ of 12.6 kcal/mol resulted in 99% ee of S isomer **7** in 99% ee of S isomer (see Table 1). The evaluated % ee values are in line with the experimental values previously recorded, with percent ee of 97% [11]. The results obtained with M06-2X and B3LYP in the gas phase and solvent phase

Table 1 Theoretically estimated % ee using Gibbs free energies when N-phenylmaleimide (**dn**) and N-(4-trifluoromethylphenyl) maleimide (**dn`**) are used as the dienophile

Dienophile	Parameters	M06-2X/6-31+G(d,p)		B3LYP/6-31+G(d,p)	
		Gas phase (kcal/mol)	Solvent phase (kcal/mol)	Gas phase (kcal/mol)	Solvent phase (kcal/mol)
dn	$\Delta G^{\neq}_{RHS}$	11.1	9.7	13.9	12.6
	$\Delta G^{\neq}_{LHS}$	7.7	7.6	11.9	11.7
	$\delta\Delta G^{\neq}$	−3.3	−2.0	−1.9	−0.8
	% ee	99	93	93	63
dn`	$\Delta G^{\neq}_{RHS}$	7.2	7.1	10.3	10.1
	$\Delta G^{\neq}_{LHS}$	12.6	12.4	13.2	13.2
	$\delta\Delta G^{\neq}$	−5.3	−5.2	−2.9	−3.0
	% ee	99	99	98	98

were largely similar and extremely close to the observed values (see Table 1).

4 Conclusion

The origin of stereo-selectivity, the reaction mechanism and the effect of substituents in the reaction between anthrone and maleimide have been figured out computationally. The factor that causes the stereo-selectivity is the difference in the type of bonding between the RHS and LHS conformers. The N–H···O interactions are stronger than the C–H···O interactions which lead to greater stability of the conformer, thereby increasing the activation energy required to proceed. Moving on to the difference observed in the formation of product caused by the difference in the substituents attached on maleimide, theoretical calculations show that on using N-phenylmaleimide, the electronic energy required to form MA is higher than for the DA formation; moreover, the DA product is energetically stable than the MA. However, when *N*-(4-trifluoromethylphenyl)maleimide is used, a reversal in product formation was observed, and this is attributed to the electron deficiency in the maleimide caused by the highly electron-withdrawing groups which inhibit the C–C coupling involved in DA reaction, thereby compelling the course of the reaction to prefer the much feasible de-protonation step leading to the formation of MA. Thus, it is worth noting that the presence of hydrogen bonding (i.e. N–H···O and C–H···O) and steric orientation between the catalyst and the reacting substrates are the main factors that foster the enantioselectivity. The modification of substituents promotes such interactions, thereby playing a decisive role in shaping the stereo-chemical path of the reaction. These findings may possibly benefit experimentalists in the design of future experiments.

Supplementary Information The online version contains supplementary material available at https://doi.org/10.1007/s00214-022-02902-9.

Declarations

Conflict of interest The authors declare no competing financial interests.

References

1. Jimenez EI, Narváez WEV, Román-Chavarría CA, Vazquez-Chavez J, Rocha-Rinza T, Hernández-Rodríguez M (2016) Bifunctional thioureas with alpha-trifluoromethyl or methyl groups: comparison of catalytic performance on Michael additions. J Org Chem. https://doi.org/10.1021/acs.joc.6b01063
2. Malerich JP, Hagihara K, Rawal VH (2008) Chiral squaramide derivatives are excellent hydrogen bond donor catalysts. J Am Chem Soc. https://doi.org/10.1021/ja805693p
3. Cinchilla R, Nájera C, Sánchez-Agulló P (1994) Enantiomerically pure guanidine-catalysed asymmetric nitroaldol reaction. Tetrahedron Asymmetry. https://doi.org/10.1016/0957-4166(94)80183-5
4. Curran DP, Kuo LH (1994) Acceleration of a Dipolar claisen rearrangement by hydrogen bonding to a soluble diaryl urea. J Org Chem. https://doi.org/10.1016/00404-0399(50)1394-W
5. Schreiner PR (2003) Metal-free organocatalysis through explicit hydrogen bonding interactions. Chem Soc Rev. https://doi.org/10.1039/B107298F
6. Zhang Z, Schreiner PR (2009) (Thio)urea organocatalysis—what can be learnt from anion recognition? Chem Soc Rev. https://doi.org/10.1039/B801793J
7. Bernardi L, Fochi M, Franchini MC, Ricci A (2012) Bioinspired organocatalytic asymmetric reactions. Org Biomol Chem. https://doi.org/10.1039/C2OB07037E
8. Okino T, Hoashi Y, Takemoto Y (2003) Enantioselective michael reaction of malonates to nitroolefins catalyzed by bifunctional organocatalysts. J Am Chem Soc. https://doi.org/10.1021/ja036972z
9. Sun YL, Wei Y, Shi M (2017) Applications of chiral thiourea-amine/phosphine organocatalysts in catalytic asymmetric reactions. ChemCatChem. https://doi.org/10.1002/cctc.201601144
10. Agarwal J (2016) Progress in amino sugars derived asymmetric organocatalysis. Org Biomol Chem. https://doi.org/10.1039/C6OB01462C
11. Zea A, Valero G, Alba AR, Moyano A, Riosa R (2010) Bifunctional thiourea-catalyzed asymmetric addition of anthrones to maleimides. Adv Synth Catal. https://doi.org/10.1002/adsc.201000031
12. Maliekal PJ, Gulvi NR, Karnik AV, Badani PM (2020) Origin and turnaround of enantioselectivity in a chiral organocatalysed Diels–Alder reaction: a mechanistic study. J Phys Org Chem. https://doi.org/10.1002/poc.4072
13. Steiner T (2003) C–H¨¨O hydrogen bonding in crystals. Crystallogr Rev. https://doi.org/10.1080/08893110310001621772
14. Itoh Y, Nakashima Y, Tsukamoto S, Kurohara T, Suzuki M, Sakae Y, Oda M, Okamoto SY (2019) N^{+}–C–H···O hydrogen bonds in protein–ligand complexes. Sci Rep. https://doi.org/10.1038/s41598-018-36987-9
15. Frisch MJ, Trucks GW, Schlegel HB, Scuseria GE, Robb MA, Cheeseman JR, Scalmani G, Barone V, Mennucci B, Petersson GA, Nakatsuji H, Caricato M, Li X, Hratchian HP, Izmaylov AF, Bloino J, Zheng G, Sonnenberg JL, Hada M, Ehara M, Toyota K, Fukuda R, Hasegawa J, Ishida M, Nakajima T, Honda Y, Kitao O, Nakai H, Vreven T, Montgomery JA Jr, Peralta JE, Ogliaro F, Bearpark M, Heyd JJ, Brothers E, Kudin KN, Staroverov VN, Kobayashi R, Normand J, Raghavachari K, Rendell A, Burant JC, Iyengar SS, Tomasi J, Cossi M, Rega N, Millam NJ, Klene M, Knox JE, Cross JB, Bakken V, Adamo C, Jaramillo J, Gomperts R, Stratmann RE, Yazyev O, Austin AJ, Cammi R, Pomelli C, Ochterski JW, Martin RL, Morokuma K, Zakrzewski VG, Voth GA, Salvador P, Dannenberg JJ, Dapprich S, Daniels AD, Farkas Ö, Foresman JB, Ortiz JV, Cioslowski J, Fox DJ (2009) Gaussian 09, Revision A. Gaussian, Inc., Wallingford
16. Krishnan R, Binkley JS, Seeger R, Pople JA (1980) Self-consistent molecular orbital methods. XX. A basis set for correlated wave functions. J Chem Phys. https://doi.org/10.1063/1.438955
17. Lee C, Yang W, Parr RG (1988) Development of the Colic-Salvetti correlation-energy formula into a functional of the electron density. Phys Rev B. https://doi.org/10.1103/PhysRevB.37.785

18. Fernando RC, Houk KN (2004) Computational evidence for the enamine mechanism of intramolecular aldol reactions catalyzed by proline. Angew Chem Int Ed. https://doi.org/10.1002/anie.200460916
19. Becke AD (1993) Density-functional thermochemistry. III. The role of exact exchange. J Chem Phys. https://doi.org/10.1063/1.464913
20. Exploring chemistry with electronic structure methods third edition (2015)
21. Lam Y, Houk KN (2015) Origins of stereoselectivity in intramolecular aldol reactions catalyzed by cinchona amines. J Am Chem Soc. https://doi.org/10.1021/ja513096x
22. Simon L, Goodman JM (2011) How reliable are DFT transition structures? Comparison of GGA, hybrid-meta-GGA and meta-GGA functionals. Org Biomol Chem. https://doi.org/10.1039/C0OB00477D
23. Krenske EH, Houk KN (2013) Aromatic interactions as control elements in stereoselective organic reactions. Acc Chem Res. https://doi.org/10.1021/ar3000794
24. Linder M, Brinck T (2013) On the method-dependence of transition state asynchronicity in Diels–Alder reactions. Phys Chem Chem Phys. https://doi.org/10.1039/c3cp44319a
25. Walker M, Andrew JA, Sen A, Dessent CEHD (2013) Performance of M06, M06-2X, and M06-HF density functionals for conformationally flexible anionic clusters: M06 functionals perform better than B3LYP for a model system with dispersion and ionic hydrogen-bonding interactions. J Phys Chem A. https://doi.org/10.1021/jp408166m
26. Atalay A, Abbasoglu R (2018) Theoretical investigation on facial and stereoselectivity in Diels–Alder cycloadditions of maleic anhydride to dissymmetric cage-annulated cyclohexa-1,3-dienes. J Phys Org Chem. https://doi.org/10.1002/poc.3893
27. Katarzyna S, Nödling AR, Tsai Y, Luk LYP, Moliner V (2018) The Reaction mechanism of organocatalytic michael addition of nitromethane to cinnamaldehyde: a case study on catalyst regeneration and solvent effect. J Phys Chem A. https://doi.org/10.1021/acs.jpca.7b11803
28. Sastre S, Casasnovas R, Munoz F, Frau J (2013) Isodesmic reaction for pK_a calculations of common organic molecules. Theor Chem Acc. https://doi.org/10.1007/s00214-012-1310-z
29. Patel P, Lingayat S, Gulvi N, Badani P (2018) Mechanistic and kinetic insights of reduction of indophenol by sodium borohydride: a theoretical study to explore the effect of solvent and counter ion. Chem Phys. https://doi.org/10.1016/j.chemphys.2018.02.021
30. Gulvi N, Patel P, Badani PM (2018) Exploring unimolecular dissociation kinetics of ethyl dibromide through electronic structure calculations. Chem Phys. https://doi.org/10.1016/j.chemphys.2018.03.018
31. Balci M (2005) Basic 1H- and 13C-NMR spectroscopy. Elsevier Science
32. Pinjari V, Gejji SP (2008) Electronic structure, molecular electrostatic potential, and NMR chemical shifts in cucurbit[n]urils (n = 5–8), ferrocene, and their complexes. J Phys Chem. https://doi.org/10.1021/jp809293s
33. Glendening ED, Landis CR, Weinhold F (2012) Natural bond orbital methods. WIREs Comput Mol Sci. https://doi.org/10.1002/wcms.51
34. Rozas I (2007) On the nature of hydrogen bonds: an overview on computational studies and a word about patterns. Phys Chem Chem Phys. https://doi.org/10.1039/b618225a
35. Shchavlev AE, Pankratov SAV (2006) DFT computational studies on rotation barriers, tautomerism, intramolecular hydrogen bond, and solvent effects in 8-hydroxyquinoline. Int J Quantum Chem. https://doi.org/10.1002/qua.20759
36. Linder M, Brinck T (2012) Stepwise Diels–Alder: more than just an oddity? A computational mechanistic study. J Org Chem. https://doi.org/10.1021/jo301176t
37. Domingo LR, Ríos-Gutiérrez M, Pérez P (2016) Applications of the conceptual density functional theory indices to organic chemistry reactivity. Molecules. https://doi.org/10.3390/molecules21060748
38. Domingo LR, Sáez JA (2009) Understanding the mechanism of polar Diels–Alder reactions. Org Biomol Chem. https://doi.org/10.1039/B909611F
39. Clayden J, Greeves N, Warren SG (2012) Organic chemistry. Oxford University Press, Oxford
40. Chakraborty S, Saha C (2016) The Curtin-Hammett principle a qualitative understanding. J Sci Educ. https://doi.org/10.1007/s12045-016-0307-7
41. Raghavan BS (2016) Transition state models for understanding the origin of chiral induction in asymmetric catalysis. Acc Chem Res. https://doi.org/10.1021/acs.accounts.6b00053